

The Fe II excitation mechanism in KQ Puppis

A. Redfors¹ and S.G. Johansson²

¹ Kristianstad University, 291 88 Kristianstad, Sweden

² Lund University, Physics Department, Atomic Spectroscopy, Box 118, 221 00 Lund, Sweden

Received 23 June 2000 / Accepted 22 September 2000

Abstract. We discuss different excitation processes behind the Fe II emission lines in the IUE spectrum of KQ Puppis (Boss 1985), a VV Cephei type of spectroscopic binary. Several papers have been published on the subject suggesting a number of processes behind the strong Fe II emission lines. We propose that there are two processes operating: selective photoexcitation by continuum radiation (PCR) from the B-star companion, and photoexcitation by accidental resonance (PAR) by the H Ly α radiation field. We suggest excitation channels for each of the Fe II emission lines identified in the spectrum.

Key words: atomic data – atomic processes – stars: binaries: spectroscopic – stars: individual: KQ Puppis

1. Introduction

KQ Puppis¹ is known as a bright VV Cephei variable. It was given the classification M2ep Iab + B by Bidelman (1954), who also listed it along with VV Cephei. Some ten years later Jaschek & Jaschek (1963) classified the stars as M1 Iab and B2V with the classification of the hot companion based solely on He I ($\lambda 3819$ Å). A long term spectroscopic study of the system by Cowley (1965) established the period to be 27 years and the inclination, $i \geq 45^\circ$. The orbital elements determined by Cowley (1965) are used in more recent papers, e.g. by Che & Reimers (1983), who determined the mass loss rate to $1.0 \cdot 10^{-7} M_\odot/\text{yr}$. Later Rossi et al. (1992) have proposed a tentative model of the system and thereby revised the classification of the hot companion to B0Vp. The work by Rossi et al. (1992) provides further basic stellar data on KQ Puppis, such as mass ratio, interstellar extinction and distance.

Spectral analyses of KQ Puppis have been reported in several papers (McLaughlin 1948; Bosman-Crespin & Swensson 1956; Jaschek & Jaschek 1963; Cowley 1965; Swings 1969; Altamore et al. 1982; Che & Reimers 1983; Altamore et al. 1992; Rossi et al. 1992; Muratorio et al. 1992).

The early observations (UV and visible) are summarized by Cowley (1965) and Swings (1969). They propose the presence

of a shell spectrum (1947–49) with sharp absorption and emission features of ionized iron group elements such as Sc II, Ti II, Cr II, Fe II, and Ni II. The spectral lines have intensities that vary with time, increasing towards periastron. However, the intensity periodicity is suggested to be less pronounced than in the case of VV Cep. The forbidden emission lines of KQ Puppis, e.g. [Fe II], are observed to have more or less constant intensities. These lines are therefore suggested to originate in a tenuous, gaseous region enveloping the stars. Broad and hazy absorption features associated with the hot companion were difficult to evaluate in these early observations.

Altamore et al. (1982) published a list of line identifications based on high resolution spectra from the International Ultraviolet Explorer (IUE). The spectra which were observed in 1979 and 1980, cover the region 1190 – 3228 Å, and coincide with the resonance region of singly ionized iron group elements (Johansson & Cowley 1988). Altamore et al. (1982) confirm the findings of earlier observations and conclude that at least two line systems exist, viz. a broad absorption line system of multiply ionized species from the vicinity of the B star and a sharp line system of neutral and singly ionized elements originating from an extended envelope. They also found that absorption and emission features of the sharp line system have a radial velocity difference of about 40 km/s, and claimed the presence of Fe II emission lines originating from levels as high as 13 eV above the ground state. Che & Reimers (1983) discuss the Fe II spectrum in KQ Puppis in some detail and observe emission in a number of UV multiplets, see discussion in Sect. 3.

Three sequential papers following up the line identification list of Altamore et al. (1982) appeared in 1992. 1) “An atlas of the optical and the ultraviolet spectrum” (Altamore et al. 1992); 2) “A possible model” (Rossi et al. 1992) and 3) “A discussion of the Fe II spectrum, level population and spectral synthesis” (Muratorio et al. 1992). Muratorio et al. (1992) present a model for Fe II in which they use different Boltzmann excitation functions for levels having excitation energies below and above 8 eV. However, the conclusion in the paper is that Fe II levels below 8 eV are populated according to a mean excitation temperature of about 9000 K whereas the population excess of levels above 8 eV could be due to dielectronic recombination. Muratorio et al. (1992) claim that the main source of scatter of the obser-

Send offprint requests to: A. Redfors

¹ Boss(1985), HR 2902, HD60414-60415

vational data in their model is caused by uncertainties in the atomic data.

In the present work we have looked through high resolution IUE spectra and we discuss excitation processes for all identified Fe II emission lines. We use the designations PCR for photoexcitation by continuum radiation and PAR for photoexcitation by accidental resonances. PCR is used for a process where photons of the continuum radiation give rise to selective photoexcitation in a species (Johansson & Hamann 1993). PAR is a designation for the Bowen mechanism, and was introduced by Kastner & Bhatia (1986). It is used for a process where a strong emission feature from one species coincides in wavelength with a transition in another species. If the lower level of this later transition is populated, photons can be absorbed, and the photoexcited level decays in one or more fluorescence channels. Both processes normally result in a flux redistribution towards longer wavelengths.

2. The observations

The spectra used in this analysis are from the IUE archives. Two of them (SWP 4284 and LWR 3787), presented in the atlas of Altamore et al. (1992), were recorded in February 1979, when the binary phase, according to Cowley (1965), was 0.24. This means that the hot companion star is at the far side of the M star, but not obscured. We also used IUE spectrum LWP 23 117 above 3100 Å, recorded by De Martino on 17 May 1992. This spectrum is recorded at a different binary phase and shows a smaller shift between the Fe II absorption and emission features.

For the observation at different phases we have only been interested in the wavelength shifts that are due to the relative motion of the stars and not those that are due to the radial velocity of the binary system. The wavelength scale for the observed spectra is therefore calibrated using sharp, apparently unblended, Fe II absorption lines. The Fe II laboratory wavelengths used for the calibration are all from Fourier Transform Spectroscopy (FTS) measurements and are in every case the most accurate value available. Wavelengths given with five decimal places are published in: Nave et al. (1991) for $\lambda > 2000$ Å and Nave et al. (1997) for $\lambda < 2000$ Å. The remaining Wavelengths are from an unpublished list of preliminary Fe II wavelengths by Johansson.

3. The Fe II spectrum

Fe II is, as discussed above, present with sharp absorption and emission features in the investigated IUE spectra of KQ Puppis, and is by far the most prominent of the iron spectra. This is partly explained by the fact that the strong Fe II resonance lines fall in the IUE region, whereas resonance lines of Fe I and Fe III fall in the visible and well below the lower wavelength limit of IUE, respectively.

In this work we have chosen to concentrate on the Fe II lines and their excitation mechanisms. There are different line shapes for the Fe II lines, ranging from pure absorption to pure emission through P-Cygni character of various degrees. We observe that

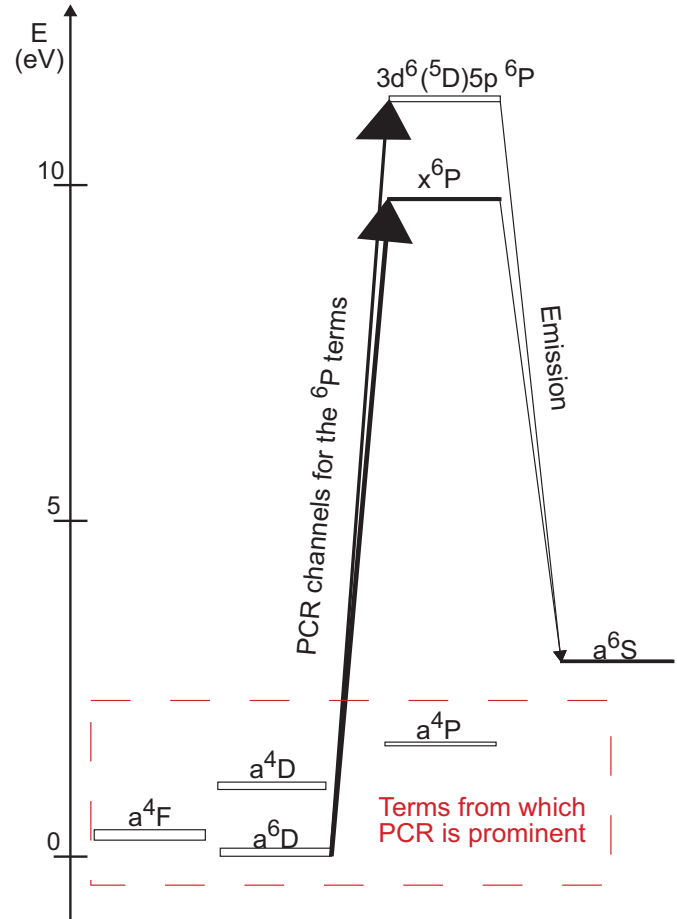


Fig. 1. Two examples of photoexcitation by continuum radiation (PCR) from the ground term of Fe II. Terms from which PCR is prominent in KQ Puppis are marked.

lines with small gf values appear in emission but seldom in absorption. Lines with larger gf values appear with any of the three profiles depending on the level population. We concentrate on pure emission lines and do not discuss the P-Cygni type profiles.

A pure blackbody intensity distribution for $T = 30000$ K peaks at around 1000 Å. The main part of the continuum radiation from the hot companion star ($T_{\text{eff}} = 30000$ K) is therefore emitted in the region of the Fe II resonance lines. This led us to the hypothesis that photoexcitation by continuum radiation (PCR), see Fig. 1, is the dominating excitation process for the observed Fe II emission lines in KQ Puppis.

We have looked through the IUE spectra of KQ Puppis in detail, and all Fe II emission lines identified are presented in Tables 1 – 4. For each of the lines we give the laboratory wavelength and a wavelength shift, which is the difference between the measured position of an emission feature relative to the wavelength scale defined by absorption lines, see Sect. 2. We also give the excitation potential for the upper level and the photoexcitation channels, e.g. $a^6D - x^6P$ in Fig. 1. Excitation channels with wavelengths below the lower limit of IUE ($\lesssim 1200$ Å) are proposed, but have evidently not been observed.

Wavelengths in Table 1 above 3100 Å are from the observation LWP 23117 recorded at a different phase. The wavelength shift between absorption and emission features is smaller in LWP 23117.

The PCR emission lines in KQ Puppis are formed through the absorption of continuum radiation in the Fe II resonance region. All absorption lines that are expected to be present, based on oscillator strengths and lower level excitation potential and population, are observed and all the observed PCR lines are given in Tables 1 and 2. We have found no inconsistencies with the idea of PCR as the dominating excitation process. The other processes forming Fe II emission lines is the PAR by H Ly α (Table 3) and secondary fluorescence (Table 4).

We have found absorption lines from levels up to around 2.0 eV, where the $3d^7 a^2G$ levels are barely populated. The weak emission lines at $\lambda\lambda 2982, 2997$ Å ($b^2D - y^2F$) appear as fluorescence due to the $a^2G - y^2F$ PCR process. Levels above 2.0 eV appear not to have a thermal population sufficient to give rise to absorption lines. However, there is one term (b^4F) at 2.8 eV that shows absorption, but this term (b^4F) we propose to be populated by fluorescence from x^4D, y^4D and z^4G , see Table 1. Furthermore, a high 4G term ($(^4G)4s4p(^1P) ^4G$) is populated from this b^4F term. All the strong (diagonal) lines of this $b^4G - (^4G)4s4p(^1P) ^4G$ multiplet are observed, and this suggests a broad PCR process. Notice, that the somewhat unexpected population of the b^4F term leads to emission from this high 4G state. There could be other excitation channels involved in this, but we have not been able to establish any.

The emission lines within multiplets UV 193 and UV 191 appear with different relative intensities, see Fig. 2. The intensities are expected to be proportional to $2J + 1$ for the upper 6P levels. In UV 193 the intensities are reversed with the line having the largest J (1473 Å) being the weakest, but this is not unusual for this multiplet, as it has also been seen in laboratory spectra. In UV 191 the $\lambda 1785$ and 1786 Å lines appear to be equally strong and the $\lambda 1788$ Å line is almost missing. However, this can be explained by the $\lambda 1785$ Å being saturated and that the $\lambda 1788$ Å is perturbed by both a Ni II absorption line and an IUE reseau mark. Notice also that the parasite line to UV 191 discussed in Johansson et al. (1995) does not appear in the tables. This line is not resolved in the IUE spectrum.

We have chosen to treat emission multiplets having a^4D or a^4P as the lower term separately and present them in Table 2. These lines have pure emission profiles, in spite of a large population of the lower levels. It is the relatively small gf values for these transitions that give rise to the pure emission profiles. The upper levels of these transitions in Table 2 are consequently populated by photoexcitation from “another” of the four lowest terms, but in some cases also by cascading from e^4D and e^6D , see Table 2.

A third category of emission lines are presented in Table 3. These are the H Ly α PAR process lines. H Ly α pumps the upper levels of the three transitions in Table 3. The $\lambda 1869.5$ Å line is produced by pumping from a^4G into the high (a^2F) $4s4p(^3P) ^4G$ state. This process was first described in Johansson & Jordan (1984) where the process enabled the authors to establish

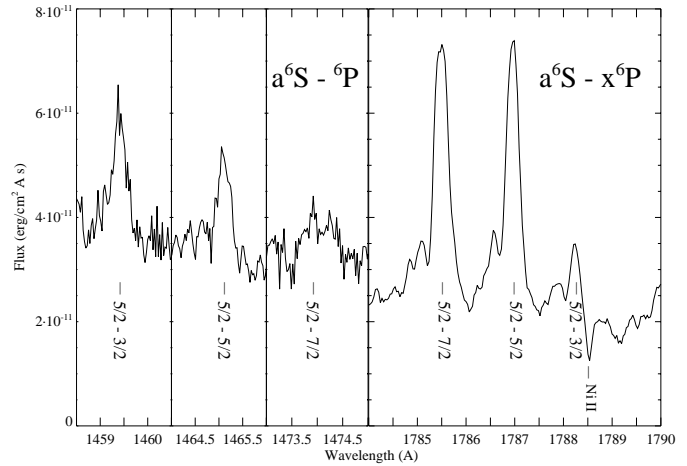


Fig. 2. Relative intensities of the lines in UV 193 and UV 191. See discussion in text.

the (a^2F) $4s4p(^3P) ^4G$ term. The strong emission line $z^4F_{9/2} - b^4G_{11/2}$ ($\lambda 9997.56$ Å) was later suggested by Johansson (1990) to be a secondary fluorescence and thus a confirmation of this process. See also Judge et al. (1992) and references therein for a detailed discussion of Fe II excitation mechanisms for low gravity cool stars.

The second H Ly α PAR process is the pumping of the mixed $3d^6(^5D) 5p ^6F_{9/2}$ and $3d^6(b^3F)4p ^4G_{9/2}$ levels from $a^4D_{7/2}$ (Johansson & Jordan 1984), which gives two fluorescence lines, $\lambda 2506.8$ and 2508.3 Å, see Fig. 3. The $a^4D_{7/2} - 3d^6(^5D)5p ^6F_{9/2}$ ($\lambda 1217.9$ Å) pump channel is in closer resonance with H Ly α than the $a^4D_{7/2} - 3d^6(b^3F)4p ^4G_{9/2}$ ($\lambda 1218.2$ Å), see Fig. 3. This favors the $c^4F_{7/2} - 3d^6(^5D)5p ^6F_{9/2}$ ($\lambda 2506.8$ Å) fluorescence line. However, in KQ Puppis both emission lines have about the same intensity even though the $\lambda 2506.8$ Å feature in the spectrum is blended with an emission component of UV 175, see Table 1. This shows that the width of Ly α in KQ Puppis is large enough to encompass both ($\lambda 1217.9$ and 1218.2 Å) excitation channels, see Fig. 3.

The fourth category of emission lines, presented in Table 4, is secondary fluorescence lines. These emission lines from the e^4D, e^6D terms are often appearing in astrophysical spectra, and they are also present in the case of KQ Puppis. We suggest an explanation for the presence of these secondary fluorescence lines based on two different schemes. Many of the $3d^6(^5D)5p$ levels have strong absorption channels around 1000 Å from the ground term and from the lowest quartet terms. This is the wavelength region where the continuum radiation peaks, and we suggest that PCR from these low terms are populating the $3d^6(^5D)5p$ levels. Levels of the e^4D, e^6D terms are then populated by the normally strong IR transitions from these $3d^6(^5D)5p$ levels, see Table 4. The other scheme that is adding to the population of the e^4D, e^6D levels is selective in J . Levels with J -values 7/2 and 9/2 are populated by emission from $3d^6(^5D)5p ^6F_{9/2}$, which is populated by PAR, as discussed above.

Table 1. Fe II PCR emission lines. $\Delta\lambda$ is the difference between the observed emission wavelength and the wavelength scale of the sharp absorption lines. Wavelengths above 2000 Å are in air.

Mult.	Transition		λ_{lab} (Å)	$\Delta\lambda$ (Å)	E_{up} (eV)	Major PCR channels		λ_{lab} (Å)
UV 193 ^a	$a^6S_{5/2}$	–	$3d^6(^5D)5p\ ^6P_{3/2}$	1459.30341	0.09	11.4	$a^6D_{5/2}$ – $^6P_{3/2}$ $a^6D_{3/2}$ – $^6P_{3/2}$ $a^6D_{1/2}$ – $^6P_{3/2}$	1096.78234 1099.13224 1100.51649
193 ^a	$a^6S_{5/2}$	–	$^6P_{5/2}$	1465.04029	0.05	11.4	$a^6D_{7/2}$ – $^6P_{5/2}$ $a^6D_{5/2}$ – $^6P_{5/2}$ $a^6D_{3/2}$ – $^6P_{5/2}$	1096.60723 1100.01978 1102.38359
193 ^a	$a^6S_{5/2}$	–	$^6P_{7/2}$	1473.83292	0.07	11.3	$a^6D_{9/2}$ – $^6P_{7/2}$ $a^6D_{7/2}$ – $^6P_{7/2}$ $a^6D_{5/2}$ – $^6P_{7/2}$	1096.8709 1101.52612 1104.9681
191	$a^6S_{5/2}$	–	$x^6P_{7/2}$	1785.2777	0.21	9.8	$a^6D_{9/2}$ – $x^6P_{7/2}$ $a^6D_{7/2}$ – $x^6P_{7/2}$ $a^6D_{5/2}$ – $x^6P_{7/2}$	1260.5256 1266.67971 1271.23504
191	$a^6S_{5/2}$	–	$x^6P_{5/2}$	1786.75804	0.20	9.8	$a^6D_{7/2}$ – $x^6P_{5/2}$ $a^6D_{5/2}$ – $x^6P_{5/2}$ $a^6D_{3/2}$ – $x^6P_{5/2}$	1267.4158 1271.9740 1275.1436
191	$a^6S_{5/2}$	–	$x^6P_{3/2}$	1788.0040 ^b	0.24	9.8	$a^6D_{5/2}$ – $x^6P_{3/2}$ $a^6D_{3/2}$ – $x^6P_{3/2}$ $a^6D_{1/2}$ – $x^6P_{3/2}$	1272.6310 1275.7920 1277.6585
	$b^4G_{5/2}$	–	$(^4G)4s4p(^1P)\ ^4G_{5/2}$	1839.8079 ^c	0.24	13.5	$b^4F_{3/2}^d$ – $^4G_{5/2}$	1168.2519
	$b^4G_{7/2}$	–	$^4G_{7/2}$	1840.00058 ^c	0.15	13.5	$b^4F_{5/2}^d$ – $^4G_{7/2}$	1166.9631
	$b^4G_{9/2}$	–	$^4G_{9/2}$	1841.7091	0.26	13.5	$b^4F_{7/2}^d$ – $^4G_{9/2}$	1166.0352
	$b^4G_{11/2}$	–	$^4G_{11/2}$	1843.2610	0.20	13.4	$b^4F_{9/2}^d$ – $^4G_{11/2}$	1164.8660
	$c^4F_{9/2}$	–	$u^4F_{9/2}$	2307.3129	0.20	11.6	$a^4F_{9/2}$ – $u^4F_{9/2}$ $a^4F_{7/2}$ – $u^4F_{9/2}$ $a^4D_{7/2}$ – $u^4F_{9/2}$	1091.5597 1098.2545 1169.1902
	$c^4F_{7/2}$	–	$u^4F_{7/2}$	2308.7667	0.19	11.6	$a^4F_{9/2}$ – $u^4F_{7/2}$ $a^4F_{7/2}$ – $u^4F_{7/2}$ $a^4D_{5/2}$ – $u^4F_{7/2}$	1091.5276 1098.2103 1175.1426
	$c^4F_{5/2}$	–	$u^4F_{5/2}$	2311.2251	0.21	11.6	$a^4F_{7/2}$ – $u^4F_{5/2}$ $a^4F_{5/2}$ – $u^4F_{5/2}$ $a^4D_{3/2}$ – $u^4F_{5/2}$	1099.3200 1104.2714 1180.4258
	$c^4F_{3/2}$	–	$u^4F_{3/2}$	2311.2891	0.15	11.6	$a^4F_{3/2}$ – $u^4F_{3/2}$ $a^4D_{1/2}$ – $u^4F_{3/2}$	1108.5115 1183.6883
179	$b^4F_{3/2}$	–	$x^4D_{1/2}$	2466.67133	0.40	7.9	$a^4F_{3/2}$ – $x^4D_{1/2}$	1654.47854
179	$b^4F_{5/2}$	–	$x^4D_{3/2}$	2466.81942	0.25	7.9	$a^4F_{5/2}$ – $x^4D_{3/2}$ $a^4F_{3/2}$ – $x^4D_{3/2}$	1649.4262 1657.0660
179	$b^4F_{7/2}$	–	$x^4D_{5/2}$	2470.66944	0.32	7.8	$a^4F_{7/2}$ – $x^4D_{5/2}$ $a^4F_{5/2}$ – $x^4D_{5/2}$	1643.57878 1654.6683
179	$b^4F_{5/2}$	–	$x^4D_{5/2}$	2478.57218	0.32	7.8	”	”
179	$b^4F_{3/2}$	–	$x^4D_{5/2}$	2484.24463	0.33	7.8	”	”
179	$b^4F_{9/2}$	–	$x^4D_{7/2}$	2480.15766	0.28	7.8	$a^4F_{9/2}$ – $x^4D_{7/2}$	1637.39972
179	$b^4F_{7/2}$	–	$x^4D_{7/2}$	2490.85840	0.27	7.8	”	”
175	$b^4F_{5/2}$	–	$y^4D_{3/2}$	2497.81926	0.22	7.8	$a^4F_{5/2}$ – $y^4D_{3/2}$ $a^4F_{3/2}$ – $y^4D_{3/2}$	1663.22299 1670.99111
175	$b^4F_{7/2}$	–	$y^4D_{5/2}$	2506.79683	0.22 ^{bl}	7.8	$a^4F_{7/2}$ – $y^4D_{5/2}$ $a^4F_{5/2}$ – $y^4D_{5/2}$	1659.48296 1670.7912
175	$b^4F_{9/2}$	–	$y^4D_{7/2}$	2557.5060	0.28	7.7	$a^4F_{9/2}$ – $y^4D_{7/2}$ $a^4F_{7/2}$ – $y^4D_{7/2}$	1670.7470 1686.45647

Table 1. (continued)

Mult.	Transition		λ_{lab} (Å)	$\Delta\lambda$ (Å)	E_{up} (eV)	Major PCR channels		λ_{lab} (Å)
190	a ⁶ S _{5/2}	– y ⁶ P _{7/2}	2572.9679	0.22	7.7	a ⁶ D _{9/2}	– y ⁶ P _{7/2}	1608.4609
						a ⁶ D _{7/2}	– y ⁶ P _{7/2}	1618.4678
						a ⁶ D _{5/2}	– y ⁶ P _{7/2}	1625.91222
190	a ⁶ S _{5/2}	– y ⁶ P _{5/2}	2581.1107	0.24	7.7	a ⁶ D _{7/2}	– y ⁶ P _{5/2}	1621.68517
						a ⁶ D _{5/2}	– y ⁶ P _{5/2}	1629.15924
						a ⁶ D _{3/2}	– y ⁶ P _{5/2}	1634.34948
171	b ⁴ F _{9/2}	– z ⁴ G _{7/2}	2608.8528	0.28	7.6	a ⁴ F _{9/2}	– z ⁴ G _{7/2}	1692.4974
						a ⁴ F _{7/2}	– z ⁴ G _{7/2}	1708.62366
						a ⁴ F _{5/2}	– z ⁴ G _{7/2}	1720.6137
171	b ⁴ F _{7/2}	– z ⁴ G _{7/2}	2620.6951	0.31	7.6	”	”	”
171	b ⁴ F _{5/2}	– z ⁴ G _{7/2}	2629.5883	0.31	7.6	”	”	”
171	b ⁴ F _{9/2}	– z ⁴ G _{9/2}	2619.0739	0.30	7.5	a ⁴ F _{9/2}	– z ⁴ G _{9/2}	1696.79493
						a ⁴ F _{7/2}	– z ⁴ G _{9/2}	1713.00044
171	b ⁴ F _{5/2}	– z ⁴ G _{5/2}	2623.7252	0.26	7.6	a ⁴ F _{7/2}	– z ⁴ G _{5/2}	1706.1419
						a ⁴ F _{5/2}	– z ⁴ G _{5/2}	1718.10230
						a ⁴ F _{3/2}	– z ⁴ G _{5/2}	1726.39278
171	b ⁴ F _{9/2}	– z ⁴ G _{11/2}	2631.60854	0.29	7.5	a ⁴ F _{9/2}	– z ⁴ G _{11/2}	1702.0453
427	d ² F _{5/2}	– u ² G _{7/2}	2649.4693	0.26	11.5	a ⁴ F _{9/2}	– u ² G _{7/2}	1102.1601
						a ⁴ D _{5/2}	– u ² G _{7/2}	1187.4978
427	d ² F _{7/2}	– u ² G _{9/2}	2682.5107	0.27	11.4	a ⁴ F _{9/2}	– u ² G _{9/2}	1107.4304
						a ⁴ D _{7/2}	– u ² G _{9/2}	1187.4146
218	b ² P _{3/2}	– y ⁴ D _{5/2}	2709.0560	0.4bl	7.8	a ⁴ F _{7/2}	– y ⁴ D _{5/2}	1659.48296
						a ⁴ F _{5/2}	– y ⁴ D _{5/2}	1670.7912
218	b ² P _{1/2}	– y ⁴ D _{3/2}	2774.6860	0.27	7.8	a ⁴ F _{5/2}	– y ⁴ D _{3/2}	1663.22299
						a ⁴ F _{3/2}	– y ⁴ D _{3/2}	1670.99111
416	c ⁴ P _{1/2}	– v ⁴ D _{3/2}	2669.9331	0.25	10.7	a ⁴ P _{3/2}	– v ⁴ D _{3/2}	1372.2804
						a ⁴ P _{1/2}	– v ⁴ D _{3/2}	1376.66992
416	c ⁴ P _{3/2}	– v ⁴ D _{3/2}	2699.2023	0.3	10.7	”	”	”
416	c ⁴ P _{1/2}	– v ⁴ D _{1/2}	2681.0438	0.27	10.7	a ⁴ P _{1/2}	– v ⁴ D _{1/2}	1379.61258
416	c ⁴ P _{3/2}	– v ⁴ D _{5/2}	2682.9963	0.28	10.7	a ⁴ P _{5/2}	– v ⁴ D _{5/2}	1364.38360
						a ⁴ P _{3/2}	– v ⁴ D _{5/2}	1368.0812
416	c ⁴ P _{5/2}	– v ⁴ D _{7/2}	2722.7402	0.29	10.7	a ⁴ P _{5/2}	– v ⁴ D _{7/2}	1361.3594
417	c ⁴ F _{9/2}	– v ⁴ D _{7/2}	2718.6410	0.27	10.8	a ⁴ P _{5/2}	– v ⁴ D _{7/2}	1361.3594
417	c ⁴ F _{7/2}	– v ⁴ D _{5/2}	2732.9396	0.3	10.8	a ⁴ P _{5/2}	– v ⁴ D _{5/2}	1364.38360
						a ⁴ P _{3/2}	– v ⁴ D _{5/2}	1368.0812
237	b ² H _{11/2}	– y ⁴ G _{9/2}	2646.2129	0.23	7.9	a ⁴ F _{9/2}	– y ⁴ G _{9/2}	1610.92336
						a ⁴ F _{7/2}	– y ⁴ G _{9/2}	1625.52305
237	b ² H _{9/2}	– y ⁴ G _{7/2}	2652.5671	0.26	7.9	a ⁴ F _{7/2}	– y ⁴ G _{7/2}	1623.0929
						a ⁴ F _{5/2}	– y ⁴ G _{7/2}	1633.90933
237	b ² H _{9/2}	– y ⁴ G _{11/2}	2664.2004	0.24	7.9	a ⁴ F _{9/2}	– y ⁴ G _{11/2}	1612.80634
260	a ² F _{7/2}	– y ⁴ G _{7/2}	2722.0626	0.25	7.9	a ⁴ F _{7/2}	– y ⁴ G _{7/2}	1623.0929
						a ⁴ F _{5/2}	– y ⁴ G _{7/2}	1633.90933
260	a ² F _{7/2}	– y ⁴ G _{9/2}	2728.9057	0.33	7.9	a ⁴ F _{9/2}	– y ⁴ G _{9/2}	1610.92336
						a ⁴ F _{7/2}	– y ⁴ G _{9/2}	1625.52305
260	a ² F _{5/2}	– y ⁴ G _{5/2}	2741.3941	0.25	7.9	a ⁴ F _{5/2}	– y ⁴ G _{5/2}	1632.66835
						a ⁴ F _{3/2}	– y ⁴ G _{5/2}	1640.1531

Table 1. (continued)

Mult.	Transition	λ_{lab} (Å)	$\Delta\lambda$ (Å)	E_{up} (eV)	Major PCR channels	λ_{lab} (Å)
254	$a^2F_{5/2} - z^2D_{3/2}$	2897.2665	0.29	7.7	$a^4F_{5/2} - z^2D_{3/2}$ $a^4F_{3/2} - z^2D_{3/2}$	1686.6926 1694.6790
254	$a^2F_{7/2} - z^2D_{5/2}$	2959.5997	0.32	7.6	$a^4F_{7/2} - z^2D_{5/2}$ $a^4F_{5/2} - z^2D_{5/2}$	1704.6416 1716.5782
335	$b^2D_{3/2} - y^2F_{5/2}$	2982.0612	0.26	8.6	$a^2G_{7/2} - y^2F_{5/2}$	1876.8391
335	$b^2D_{5/2} - y^2F_{7/2}$	2997.2960	0.26	8.6	$a^2G_{9/2} - y^2F_{7/2}$	1860.0529
Opt 82	$b^4D_{3/2} - x^4D_{1/2}$	3105.1678	0.11 ^e	7.9	$a^4F_{3/2} - x^4D_{1/2}$	1654.4786
82	$b^4D_{1/2} - x^4D_{1/2}$	3105.5543	0.10 ^e	7.9	"	"
82	$b^4D_{3/2} - x^4D_{3/2}$	3114.2956	0.11 ^e	7.9	$a^4F_{5/2} - x^4D_{3/2}$ $a^4F_{3/2} - x^4D_{3/2}$	1649.4262 1657.0660
82	$b^4D_{1/2} - x^4D_{3/2}$	3114.6835	0.11 ^e	7.9	"	"
82	$b^4D_{5/2} - x^4D_{3/2}$	3116.5804	0.14 ^e	7.9	"	"
82	$b^4D_{5/2} - x^4D_{5/2}$	3135.3624	0.20 ^e	7.8	$a^4F_{7/2} - x^4D_{5/2}$ $a^4F_{5/2} - x^4D_{5/2}$	1643.5789 1654.6683
82	$b^4D_{7/2} - x^4D_{7/2}$	3177.5341	0.20 ^e	7.8	$a^4F_{9/2} - x^4D_{7/2}$	1637.3998

^a The “w” in w^6P was omitted by Johansson (1978) when a new lower 6P term was established.

^b This line in UV 191 is perturbed by a Ni II absorption line.

^c The lines are unresolved in the IUE spectrum.

^d The term b^4F is populated by cascading from higher levels, see text.

^e Observed wavelengths above 3100 Å are from LWP 23117 and have a smaller wavelength shift.

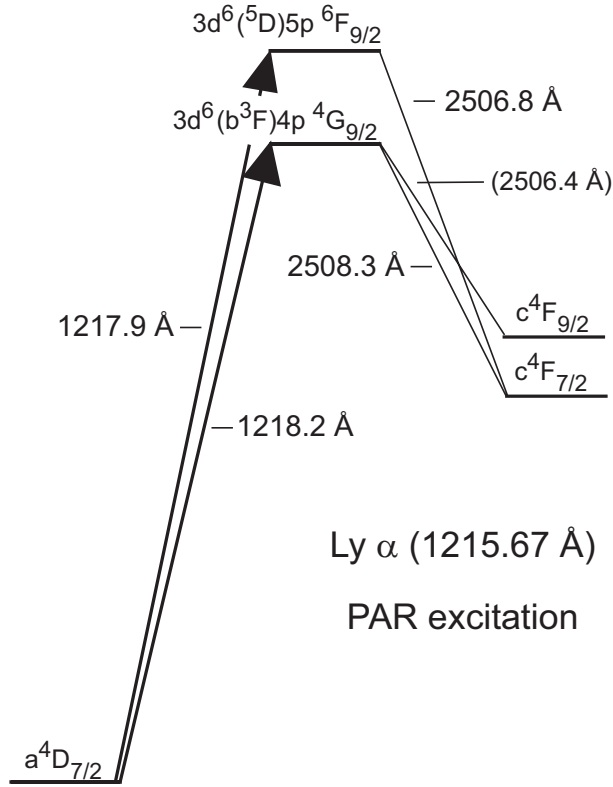


Fig. 3. H Ly α PAR process for the mixed $3d^6(^5D)5p ^6F_{9/2}$ and $3d^6(b^3F)4p ^4G_{9/2}$ from $c^4F_{7/2}$ levels.

3.1. Comments on earlier work

In this work we concentrate on Fe II, but during our analysis of the IUE spectra we have noticed that many of the lines left unclassified by Altamore et al. (1982) are due to Ni II. Nickel is next to iron the most prominent of the iron group elements in this spectrum and appears in both absorption and emission.

There is a discussion in Altamore et al. (1982) of the Mg II resonance line where the k line is claimed to be asymmetrical. The reason given is a superimposed absorption by a Fe I line at 2795.01 Å. However, this is the $a^5D_4 - z^3G_4$ transition, which is unlikely to appear in absorption. A more likely absorption in Fe I occurs at 2795.540 Å, $a^5F_4 - y^5G_3$. The Fe I λ 2795.540 Å line is the absorption part of a Mg II pumped PAR process, first proposed by Thackeray (1937). The PAR process yields primarily the 2843.976 Å and the 2823.276 Å Fe I emission lines of UV 44, see also Gahm (1974) and Johansson & Hamann (1993). However, we have not in this work been able to identify either of these PAR emission lines or other Fe I lines, not even the 2823.28 Å emission line identified by Altamore et al. (1982).

Intensity anomalies in the KQ Puppis spectrum are discussed in Muratorio et al. (1992), e.g. the strong emission lines $a^6S - x^6P$ (UV 191), $c^4F_{7/2} - (^5D)5p ^6F_{9/2}$ (2506.8 Å) and $c^4F_{7/2} - (b^3F)4p ^4G_{9/2}$ (2508.3 Å). Dielectronic recombination is proposed to enhance UV 191, whereas H Ly α pumping generates strong fluorescence in the latter two transitions. We support the latter proposal, but not the former. Dielectronic recombination has earlier been suggested as a possible explanation for the enhancement of UV 191 (Johansson & Hansen 1988),

Table 2. Fe II emission lines from the lowest odd parity levels, populated by PCR, some also by cascading from higher levels. $\Delta\lambda$ is the difference between the observed emission wavelength and the wavelength scale of the sharp absorption lines. Wavelengths above 2000 Å are in air.

Mult.	Transition		λ_{lab} (Å)	$\Delta\lambda$ (Å)	E_{up} (eV)	Major PCR channels		λ_{lab} (Å)	Cascading
UV 60	$a^4D_{7/2}$	–	$z^6F_{5/2}$	2907.8625	0.27	5.2	$a^6D_{7/2}$ – $z^6F_{5/2}$ $a^6D_{5/2}$ – $z^6F_{5/2}$ $a^6D_{3/2}$ – $z^6F_{5/2}$	2383.0605 2399.24127 2410.51919	$e^6D_{5/2}$
60	$a^4D_{5/2}$	–	$z^6F_{5/2}$	2945.2641	0.31	5.2	”	”	
60	$a^4D_{3/2}$	–	$z^6F_{5/2}$	2970.5148	0.38	5.2	”	”	
60	$a^4D_{7/2}$	–	$z^6F_{7/2}$	2916.1484	0.32	5.2	$a^6D_{9/2}$ – $z^6F_{7/2}$ $a^6D_{7/2}$ – $z^6F_{7/2}$ $a^6D_{5/2}$ – $z^6F_{7/2}$	2366.8713 2388.62890 2404.88575	$e^6D_{7/2}$
60	$a^4D_{5/2}$	–	$z^6F_{7/2}$	2953.7756	0.34	5.2	”	”	
60	$a^4D_{7/2}$	–	$z^6F_{9/2}$	2926.5859	0.35	5.2	$a^6D_{9/2}$ – $z^6F_{9/2}$ $a^6D_{7/2}$ – $z^6F_{9/2}$	2373.73566 2395.62536	
60	$a^4D_{5/2}$	–	$z^6F_{3/2}$	2939.5074	0.33	5.3	$a^6D_{5/2}$ – $z^6F_{3/2}$ $a^6D_{3/2}$ – $z^6F_{3/2}$ $a^6D_{1/2}$ – $z^6F_{3/2}$	2395.41936 2406.66125 2413.31036	
60	$a^4D_{1/2}$	–	$z^6F_{3/2}$	2979.3535	0.34	5.3	”	”	
60	$a^4D_{3/2}$	–	$z^6F_{1/2}$	2961.2730	0.35	5.3	$a^6D_{3/2}$ – $z^6F_{1/2}$ $a^6D_{1/2}$ – $z^6F_{1/2}$	2404.43100 2411.06774	
60	$a^4D_{1/2}$	–	$z^6F_{1/2}$	2975.9331	0.32	5.3	”	”	
78	$a^4P_{3/2}$	–	$z^4P_{1/2}$	2944.3951	0.34	5.9	$a^6D_{3/2}$ – $z^4P_{1/2}$ $a^6D_{1/2}$ – $z^4P_{1/2}$	2566.91263 2577.92190	
78	$a^4P_{1/2}$	–	$z^4P_{1/2}$	2964.6240	0.31	5.9	”	”	
78	$a^4P_{5/2}$	–	$z^4P_{3/2}$	2947.6549	0.36	5.9	$a^6D_{5/2}$ – $z^4P_{3/2}$ $a^6D_{3/2}$ – $z^4P_{3/2}$ $a^6D_{1/2}$ – $z^4P_{3/2}$	2563.47552 2582.58325 2593.7255	$e^4D_{5/2}$
78	$a^4P_{3/2}$	–	$z^4P_{3/2}$	2965.0323	0.35	5.9	”	”	
78	$a^4P_{1/2}$	–	$z^4P_{3/2}$	2985.5462	0.38	5.9	”	”	
78	$a^4P_{5/2}$	–	$z^4P_{5/2}$	2984.8256	0.37	5.8	$a^6D_{7/2}$ – $z^4P_{5/2}$ $a^6D_{5/2}$ – $z^4P_{5/2}$ $a^6D_{3/2}$ – $z^4P_{5/2}$	2562.53559 2591.54284 2611.0729	$e^4D_{7/2}$
78	$a^4P_{3/2}$	–	$z^4P_{5/2}$	3002.6438	0.41	5.8	”	”	
Opt 7	$a^4P_{5/2}$	–	$z^4F_{5/2}$	3163.0947	0.24 ^a	5.6	$a^4F_{7/2}$ – $z^4F_{5/2}$ $a^6D_{5/2}$ – $z^4F_{5/2}$ $a^6D_{3/2}$ – $z^4F_{5/2}$	2343.96101 2366.5938 2382.3583	$e^4D_{3/2}$
7	$a^4P_{3/2}$	–	$z^4F_{5/2}$	3183.1138	– ^b	5.5	”	”	
7	$a^4P_{5/2}$	–	$z^4F_{7/2}$	3196.0715	0.38 ^a	5.5	$a^4F_{9/2}$ – $z^4F_{7/2}$ $a^6D_{7/2}$ – $z^4F_{7/2}$ $a^6D_{5/2}$ – $z^4F_{7/2}$	2331.30840 2362.02170 2385.0061	$e^4D_{5/2}$
6	$a^4P_{3/2}$	–	$z^4D_{1/2}$	3170.3404	0.19 ^a	5.6	$a^6D_{1/2}$ – $z^4D_{1/2}$ $a^4F_{3/2}$ – $z^4D_{1/2}$	2260.2391 2375.19397	
6	$a^4P_{1/2}$	–	$z^4D_{1/2}$	3193.8009	0.10 ^a	5.6	”	”	
6	$a^4P_{5/2}$	–	$z^4D_{5/2}$	3192.9106	0.09 ^a	5.6	$a^6D_{5/2}$ – $z^4D_{5/2}$ $a^4F_{7/2}$ – $z^4D_{5/2}$	2265.9935 2360.29452	$e^4D_{5/2}$
6	$a^4P_{3/2}$	–	$z^4D_{5/2}$	3213.3093	0.29 ^a	5.6	”	”	
6	$a^4P_{1/2}$	–	$z^4D_{3/2}$	3210.4457	0.21 ^a	5.6	$a^6D_{3/2}$ – $z^4D_{3/2}$ $a^4F_{5/2}$ – $z^4D_{3/2}$	2262.6862 2368.59638	

^a Observed wavelengths above 3100 Å are from LWP 23117 and have a smaller wavelength shift, see text.

^b Expected line, but not observed. Situated in a blank spectral region.

Table 3. Fe II lines excited by H Ly α PAR process. $\Delta\lambda$ is the difference between the observed emission wavelength and the wavelength scale of the sharp absorption lines. Wavelengths above 2000 Å are in air.

Mult.	Transition	λ_{lab} (Å)	$\Delta\lambda$ (Å)	E_{up} (eV)	Population channels
$b^4G_{11/2}$	– $(a^2F)4s4p(^3P) ^4G_{11/2}$	1869.5547	0.17	13.3	H Ly α from $a^4G_{11/2}$
$c^4F_{7/2}$	– $(^5D)5p ^6F_{9/2}$	2506.79683	0.22bl	11.2	H Ly α from $a^4D_{7/2}$
$c^4F_{7/2}$	– $(b^3F)4p ^4G_{9/2}$	2508.3412	0.25	11.2	”

Table 4. Fe II lines excited by secondary fluorescence. $\Delta\lambda$ is the difference between the observed emission wavelength and the wavelength scale of the sharp absorption lines. Wavelengths above 2000 Å are in air.

Mult.	Transition	λ_{lab} (Å)	$\Delta\lambda$ (Å)	E_{up} (eV)	Population channels
UV 363	$z^6D_{9/2}$ – $(^5D)5s e^6D_{9/2}$	2537.13798	0.18	9.7	Emission from $(^5D)5p ^6P, ^6D, ^6F$
373	$z^6F_{7/2}$ – $e^6D_{5/2}$	2754.8887	0.28	9.7	”
373	$z^6F_{9/2}$ – $e^6D_{7/2}$	2767.5083	0.34bl	9.7	”
373	$z^6F_{11/2}$ – $e^6D_{9/2}$	2785.19205	0.28	9.7	”
380	$z^6P_{7/2}$ – $e^6D_{9/2}$	2839.7995	0.23	9.7	”
380	$z^6P_{5/2}$ – $e^6D_{7/2}$	2856.3772	0.17	9.7	”
391	$z^4F_{9/2}$ – $(^5D)5s e^4D_{7/2}$	2839.5130	0.29	9.8	Emission from $(^5D)5p ^4P, ^4D, ^4F, ^6F$
391	$z^4F_{7/2}$ – $e^4D_{5/2}$	2845.5949	0.26	9.9	”
391	$z^4F_{5/2}$ – $e^4D_{3/2}$	2848.3200	0.19	9.9	”
391	$z^4F_{3/2}$ – $e^4D_{1/2}$	2851.7218	0.27	10.0	”
399	$z^4D_{5/2}$ – $e^4D_{5/2}$	2848.1061	0.24	9.9	”
399	$z^4D_{7/2}$ – $e^4D_{7/2}$	2856.9090	0.32	9.8	”
Opt 181	$z^4P_{3/2}$ – $e^4D_{5/2}$	3076.4354	0.37	9.9	”
181	$z^4P_{5/2}$ – $e^4D_{7/2}$	3078.6803	0.42	9.8	”

but this is mainly to be considered for cool giants where there is no continuum radiation in the UV 9 channel. Dielectronic recombination is the inverse of autoionization, and requires in this case an adequate abundance of Fe^{2+} ions and suitable autoionizing states of Fe II. Some Fe III 4s - 4p transitions are present in the spectrum as broad absorption features with a shift of about 0.5 Å compared to the sharp features of Fe II, but the main part of the Fe III opacity is below the IUE limit (Johansson & Cowley 1988). The actual abundance of Fe^{2+} ions in the region where Fe II emission lines are formed is thereby difficult to estimate. Two autoionizing terms recombining to x^6P , with transitions around 1730 Å and 1890 Å respectively, are theoretically predicted by Johansson & Hansen (1988). The calculated wavelength from a theoretical prediction is uncertain, but recombination lines would have to appear somewhere when dielectronic recombination is an active process. However, there are no candidates in the investigated part of the KQ Puppis spectrum. For these reasons we do not support the scheme of dielectronic recombination as the population process for x^6P , but rather PCR through UV 9 as is also proposed by Che & Reimers (1983)

Che & Reimers (1983) observe emission in UV multiplets 60, 78, 191, 363, 373, 391, 399. They also claim to observe

emission in UV multiplets 375 and 384 but that has not been verified in our work. The upper term in UV 375 (e^6F) belongs to the $3d^6(^5D)4d$ subconfiguration (Johansson 1988) and we do not observe any lines in the $3d^6(^5D)4p - 3d^6(^5D)4d$ super multiplet. Only transitions in the $3d^6(^5D)4p - 3d^6(^5D)5s$ super multiplet are observed. The PCR process populating the 5p levels leads to a selective population of the $3d^6(^5D)5s$ subconfiguration.

In UV 384, as defined by Moore (1952), the upper term (e^6P) has been found to be spurious and a new identification was given by Johansson (1978). The lines from this new 6P term are not present in the IUE spectra. The paper by Che & Reimers (1983) also discusses the Fe II level population mechanism in the stellar system and propose that the systematic variation in line-profile (absorption – P-Cygni – emission) with excitation energy suggests recombination followed by cascading. They also point out the importance of the relative oscillator strengths of the different channels from a populated level. We agree in general with Che & Reimers (1983). However, we suggest, as discussed above, that all levels giving rise to emission lines are populated through photoexcitation, PCR and PAR, and that recombination is not necessary for the explanation of Fe II emission lines in KQ Puppis.

4. Summary

The ultraviolet spectrum of KQ Puppis contains a large number of Fe II emission lines, and we give wavelengths and designations for all 102 lines observed in high resolution IUE spectra. These are all pure emission line profiles. We do not discuss the more optically thick P-Cygni type transitions. We also give wavelengths and designations for 127 of the strongest PCR channels and list them with their respective emission lines. We discuss some earlier work suggesting various excitation mechanisms for Fe II in KQ Puppis, e.g. photoexcitation and dielectronic recombination. However, we propose that all of the Fe II emission lines can be explained by either selective photoexcitation by continuum radiation (PCR) from the B-star companion, or photoexcitation by accidental resonance (PAR), by the H Ly α radiation field. We also point out that these processes result in a flux redistribution towards longer wavelengths, i.e. that they are fluorescence processes.

Acknowledgements. The program at Lund on excitation mechanisms is supported by The Swedish Natural Science Research Council, The Swedish National Space Board and The Crafoord Foundation. A.R. gratefully acknowledge support from Kristianstad University.

References

- Altamore A., Giangrande A., Viotti R., 1982, A&A 49, 511
 Altamore A., Rossi C., Viotti R., Baratta G.B., 1992, A&AS 92, 685
 Bidelman W.P., 1954, ApJS 1, 175
 Bosman-Crespin D., Swensson J., 1956, Mém. Soc. R. Sci. Liège 17, 453
 Che A., Reimers D., 1983, A&A 127, 227
 Cowley A.P., 1965, ApJ 142, 299
 Gahm G.F., 1974, A&AS 18, 259
 Jaschek C., Jaschek M., 1963, PASP 75, 509
 Johansson S.G., 1978, Physica Scripta 18, 217
 Johansson S.G., 1988, In: Viotti R., Vittone A., & Friedjung M. (eds.) Physics of Formation of Fe II Lines Outside LTE. Proc. IAU Colloquium No. 94, Reidel Dordrecht, p. 13
 Johansson S.G., 1990, In: Wallerstein G. (ed.) Cool stars, Stellar systems and the Sun. ASP Conf. Ser. 9, p. 307
 Johansson S.G., Brage T., Leckrone D.S., Nave G., Wahlgren G.M., 1995, ApJ 446, 361
 Johansson S.G., Cowley C.R., 1988, JOSA B5, 2264
 Johansson S.G., Hamann F.W., 1993, Physica Scripta T47, 157
 Johansson S.G., Hansen J.E., 1988, In: Viotti R., Vittone A., & Friedjung M., (eds.) Physics of Formation of Fe II Lines Outside LTE. Proc. IAU Colloquium No. 94, Reidel, Dordrecht, p. 235
 Johansson S.G., Jordan C., 1984, MNRAS 210, 239
 Judge P.G., Jordan C., Feldman U., 1992, ApJ 384, 613
 Kastner S.O., Bhatia A.K., 1986, Comm. At. Mol. Phys. 18, 39
 McLaughlin D.B., 1948, PASP 60, 509
 Moore C.E., 1952, An Ultraviolet Multiplett Table. NBS Circular No. 488, Sect. 2
 Muratorio G., Viotti R., Friedjung M., Baratta G.B., Rossi C., 1992, A&A 258, 423
 Nave G., Learner R.M.C., Thorne A.P., Harris C.J., 1991, J. Opt. Soc. Am. B 8, 2028
 Nave G. Johansson S.G., Thorne A.P., 1997, J. Opt. Soc. Am. B 14, 1035
 Rossi C., Altamore A., Baratta G.B., Friedjung M., Viotti R., 1992, A&A 256, 133
 Swings P., 1969, Ann. d'ap. 13, 134
 Thackeray A.D., 1937, ApJ 86, 499